PAPER

Check for updates

Mechanism of Zn salt-induced deactivation of a Cu/activated carbon catalyst for low-temperature denitration *via* CO-SCR

Zhenjing Wen, [ID] [ab] Bangfu Huang,*[ab] Zhe Shi,[ab] Zhengyu Yang, [ID] [ab] Meng Dai,[ab] Wanjun Li,[ab] Gaoyong Zi[ab] and Liubin Luo[ab]

In the process of industrial flue gas denitration, the presence of heavy metals, especially Zn salts, is known to lead to the deactivation of the denitration catalysts. However, the specific mechanism of the catalyst deactivation remains unclear. In this paper, the mechanism of the $ZnCl_2$- and $ZnSO_4$-induced deactivation of low-temperature denitration catalysts in the carbon oxide (CO) selective catalytic reduction (CO-SCR) reaction was investigated using a Cu/activated carbon (AC) catalyst, in which HNO_3/AC was used as the carrier. Cu/AC, $ZnCl_2$–Cu/AC, and $ZnSO_4$–Cu/AC catalysts were prepared by the incipient wetness impregnation method. The physicochemical properties of the catalyst were examined *via* the Brunauer–Emmett–Teller method, X-ray diffraction, X-ray photoelectron spectroscopy, and Fourier transform infrared spectroscopy analyses, which proved the mechanism of catalyst denitrification and enabled the elucidation of the toxicity mechanism of the Zn salts on the Cu/AC catalyst for CO-SCR denitration at low temperatures. The results show that Zn doping reduces the physical adsorption of CO and NO and decreases the concentration of Cu^{2+} and chemisorbed oxygen (O_β), leading to the reduction of active sites and oxygen vacancies, thus inhibiting the denitration reaction. Moreover, $ZnCl_2$ is more toxic than $ZnSO_4$ because Cl^- not only occupies oxygen vacancies but also inhibits O_β migration. In contrast, SO_4^{2-} increases the surface acidity and promotes O_β supplementation. This study can provide a reference for the development of CO-SCR denitration catalysts with high resistance to Zn salt poisoning.

1 Introduction

NO_x is one of the major air pollutants emitted during fuel combustion. It causes environmental problems such as acid rain, ozone depletion, and photochemical smog, constituting a serious threat to the health of living beings on earth.[1–3] As a result of the increasingly restrictive regulations on NO_x emissions worldwide, the reduction of NO_x emissions has received extensive attention from academia and industry. Currently, selective catalytic reduction technology (SCR) is one of the most widely used methods for the effective removal of NO_x emissions from flue gas. Conventional SCR uses NH_3 as the reducing agent, which has good reducibility and catalysts with high denitration efficiency.[4,5] However, NH_3 is a costly and toxic gas whose leakage may cause serious problems, including chemical accidents, catalyst poisoning, and pipeline corrosion.[6]

To circumvent these issues, the development of new reducing agents has attracted increasing attention.

The CO has the advantages of strong reducibility, low cost, and easy availability; it can simultaneously remove CO and NO from industrial waste gas at low temperatures, which is considered as a possible technology for large-scale applications.[7–10] Unfortunately, the currently available CO-SCR denitration catalysts still present some application bottlenecks, such as low catalytic denitration capacity at low temperature, low oxidation resistance, and insufficient anti-toxicity ability against SO_2, which hinder the practical application of this technology in industry.[11] Consequently, the development of low-temperature denitration catalysts with excellent activity has become the focus of research in this field. Denitration catalysts are mainly composed of a carrier and an active component. As a catalyst carrier, activated carbon (AC) stands out because of its low cost, high content in oxygen-containing functional groups, huge specific surface area, excellent low-temperature activity, and stable chemical properties. According to a study,[12] HNO_3 activation treatment was conducted on the surface of AC, and pore volume and specific surface area were significantly increased. The increase of acidic functional groups on the surface resulted in AC having better NO_x

*a*Faculty of Metallurgical and Energy Engineering, Kunming University of Science and Technology, Kunming 650093, China. E-mail: 595762307@qq.com; 595762307@163.com

*b*Key Laboratory of Clean Metallurgy of Complex Iron Resources, Yunnan University, Kunming 650093, China

adsorption and removal ability. In addition, loading metals on AC enhance catalytic activity, and precious metals such as Pt,[13] Ru,[14] Pd,[15] Rh,[16] and Au[17] have been identified as good catalysts for CO denitration. However, precious metals have limited resources, high cost, low thermal stability, and limited development, rendering transition metals such as Fe, Ni, Co, Mn, and Cu as an attractive alternatives.[18,19] Among them, Cu has a high catalytic activity for the CO-SCR reaction and for NO_x decomposition, and different Cu species have been proved to be the active sites for NO_x adsorption.[20–22] Previous studies[23] have demonstrated the excellent performance of a Cu/AC catalyst in CO-SCR denitration; therefore, this catalyst is expected to enable the denitration process at low temperatures. However, the presence of a large amount of dust and metals (Zn, Pb, Ca, As) in the flue gas may block the catalyst pores, leading to catalyst deactivation.[24–26] Thus, the effect of heavy metals on denitration catalysts is attracting increasing research attention. In this context, Qi et al.[27] proved that Pb can reduce the amount of chemisorbed oxygen by covering the surface active sites of the catalyst, thus reducing the surface acidity and reducibility. Su et al.[28] studied the influence of Pb on a Ce–Mn/AC catalyst, finding that the selective reduction activity of the catalyst was significantly reduced after doping PbO due to the significant reduction of the total pore volume and oxygen functional groups of AC, which increased the oxide crystallization and reduced the content of Mn^{4+} and chemisorbed oxygen. Zhu[29] found that Pb doping of a 3Mn10Fe/Ni catalyst altered the content of high-valence metal elements such as Fe^{3+} and Mn^{4+}, resulting in the reduction of the lattice oxygen concentration, the performance, and the acidity of acid sites. Guo et al.[30] studied the catalytic toxicity of Zn and Pb on Mn/TiO_2, and the results showed that catalyst deactivation may be caused by the growth of TiO_2 crystals, the reduction of the redox capacity, the reduction of the surface acidity and NO adsorption energy, and the reduction of surface active substances such as Mn^{4+} and chemisorbed oxygen. Su et al.[31] investigated the influence of Zn on the deactivation and toxicity mechanism of an Mn–Ce/AC catalyst and found that doping Zn salts reduced the physical adsorption capacity of the catalyst for NH_3 and NO and increased the crystallization of Mn and Ce oxides, thereby reducing the interaction with the adsorptive gas. Meanwhile, competitive adsorption on the acidic sites of the catalyst surface was observed between Zn salts and NH_3, which resulted in a reduction of the denitration activity. However, despite the progress made in the investigation of the toxicity on catalysts, the toxicity mechanism for low-temperature CO-SCR denitration catalysts is still unclear. In particular, unveiling the mechanism of catalyst deactivation by Zn is important because Zn is one of the main components in flue gas.

Herein, to explore the toxicity mechanism of Zn salts on low-temperature CO-SCR denitration catalysts, a Cu/AC catalyst was prepared and was poisoned by $ZnCl_2$ and $ZnSO_4$, respectively. The CO-SCR denitration efficiency was studied by comparing the conversion rate of NO. The toxicity mechanism of Zn salts on the Cu/AC catalyst was studied by performing

scanning electron microscopy (SEM), energy dispersive spectroscopy (EDS), Brunauer–Emmett–Teller (BET) method, X-ray diffraction (XRD), X-ray photoelectron spectroscopy (XPS), and Fourier transform infrared (FTIR) spectroscopy analyses. The presented results can pave the way for the development of CO-SCR denitration catalysts with high resistance to Zn salt poisoning.

2 Experimental

2.1 Catalyst preparation

To prepare AC, coconut shell AC particles (coconut shell AC, particle size 10–20 mesh, Henan Gongyi Blue Sky water Purification Technology Co., Ltd) were washed with deionized water to neutral to remove ash and suspended solids, ultrasonicated in a water bath at 60 °C for 2 h, and then placed in an air-blowing drying oven at 110 °C for 24 h after pumping and filtering.[23] Then, HNO_3/AC was prepared by impregnating the as-prepared AC in an equal volume of a 30% HNO_3 solution (Zhejiang Shiping Chemical Reagent Factory), followed by refluxing for 2 h in a three-necked flask at 80 °C and drying for 24 h in a drying oven at 110 °C.[23] Three samples with a mass of 40 g HNO_3/AC were weighed using an analytical balance, and $Cu(NO_3)_2 \cdot 3H_2O$ (AR, Tianjin Kermio Chemical Reagent Co., Ltd) as the precursor was dissolved in a certain amount of deionized water and impregnated for 2 h under ultrasonic vibration at a constant temperature of 60 °C, and the samples were then drained and dried at 110 °C for 24 h. Finally, the samples were calcined under N_2 protection at 450 °C for 4 h and labeled Cu/AC. To prepare Zn-poisoned catalysts with a Zn/Cu molar ratio of 1 : 2, 52 mL $ZnCl_2$ and $ZnSO_4$ aqueous solutions were impregnated into Cu/AC catalysts and ultrasonicated for 2 h.[30,31] Then, the poisoned catalysts were drained, dried at 110 °C for 24 h, and roasted at 450 °C for 4 h under N_2 protection. The obtained samples were labeled $ZnCl_2$–Cu/AC and $ZnSO_4$–Cu/AC, respectively. The chemical composition of Cu/AC catalyst and zinc salt poisoning catalyst is shown in Table 1.

2.2 Determination of the denitration activity of the catalyst

The CO-SCR denitration experiment and Zn salt poisoning of the Cu/AC catalyst were conducted in a fixed-bed reactor. The reaction device is shown in Fig. 1. In the experiment, 8 g of catalyst sample (Cu/AC, $ZnCl_2$–Cu/AC, and $ZnSO_4$–Cu/AC, respectively) was placed in the reactor, and the reaction temperature was set by adjusting the furnace temperature, and the simulated flue gas was injected into the reactor. The

Table 1 The chemical composition of Cu/AC catalyst and zinc slats poisoning catalyst

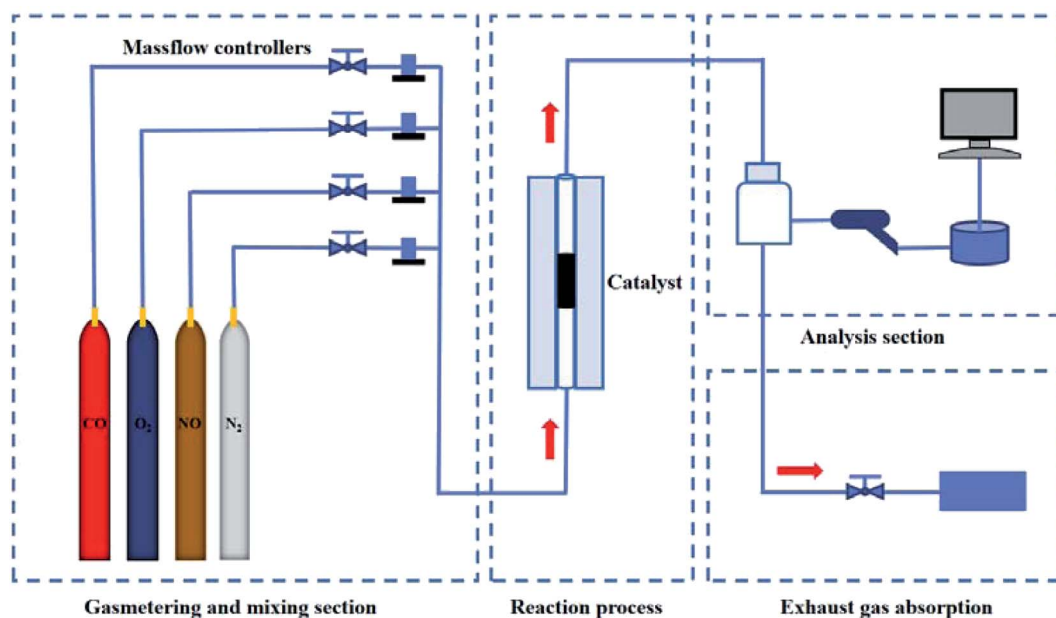| Catalysts	The mass fraction of Cu/(Cu + HNO$_3$/AC)	The molar ratio of Zn : Cu
Cu/AC	8%	1 : 2
ZnCl$_2$–Cu/AC	8%	1 : 2
ZnSO$_4$–Cu/AC	8%	1 : 2

Fig. 1 Carbonic oxide (CO) denitration experimental equipment.

simulated flue gas consisted of an NO flow rate of 4 mL min^{-1}, a CO flow rate of 40 mL min^{-1}, an O_2 volume concentration of 9%, an N_2 total flow rate of 500 mL min^{-1}, and a gas hourly space velocity of 3000 h^{-1}. The denitration tail gas was detected using a Testo-340 flue gas analyzer (German Detu Instrument Company).

The catalytic denitration activity was evaluated using NO conversion and N_2 selectivity according to the following calculation method (eqn (1) and (2)).

$$\text{NO conversion} = \left(\frac{NO_{in} - NO_{out}}{NO_{in}}\right) \times 100\% \quad (1)$$

$$N_2 \text{ selectivity} = \left(\frac{NO_{in} - NO_{out} - 2N_2O_{out}}{NO_{in} - NO_{out}}\right) \times 100\% \quad (2)$$

2.3 Catalyst characterization

The surface morphology of the catalysts was observed by SEM (Tescan VEGAS SBH). The distribution and content of metal elements on the catalyst surface were analyzed using a Tescan VEGAS SBH (EDS) device. BET/Barrett–Joyner–Halenda (BJH) experiments were performed on an N_2 adsorption and desorption tester (qds-evo). The specific surface area, pore volume, and average pore size of the catalysts were measured at 77 K according to the N_2 adsorption isotherm. XRD (TTR18 kW Cu target) was used to analyze the crystal phase pattern of the supported metal oxides. The surface atomic states of the catalysts were analyzed by XPS (PHI5000 Versaprobe-II). Al K α X-ray radiation ($hv = 1486.6$ eV) was used to measure the surface atomic states of the catalysts at 50 W, and the binding energy (BE) was calibrated using the C 1s BE value of 284.8 eV. The changes in the functional groups on the catalyst surface were investigated using an FTIR spectrometer (Nicolet iS 10) in a range of 4000–400 cm^{-1}.

3 Results and discussion

3.1 CO-SCR denitration activity

Fig. 2(a) shows the NO conversion of the Cu/AC and Zn salt-poisoned catalysts at different reaction temperatures. The Cu/AC catalyst has a high denitration rate, with the maximum NO conversion rate reaching 80% at 200 °C. When the temperature exceeds 250 °C, the reduction of denitration efficiency of Cu/AC catalyst is caused by the competitive adsorption of CO and NO. Meanwhile, the denitration rate of $ZnCl_2$–Cu/AC and $ZnSO_4$–Cu/AC decreases to 44% and 60%, respectively, at the same temperature, which suggests that $ZnCl_2$ and $ZnSO_4$ are toxic to the Cu/AC catalyst. In addition, the denitration rate of the $ZnCl_2$–Cu/AC catalyst is always lower than that of the $ZnSO_4$–Cu/AC catalyst at the same temperature, indicating that the denitration activity decays faster after $ZnCl_2$ doping. Fig. 2(b) shows the N_2 selectivity at different temperatures, which follows the order Cu/AC > $ZnSO_4$–Cu/AC > $ZnCl_2$–Cu/AC. According to a study,[31] the reason was analyzed that $ZnSO_4$ can improve the surface acidity, thereby enhancing the N_2 selectivity. The different toxicity and denitration activity of the two Zn salts is most likely caused by the difference in their constituent anions.

3.2 Surface morphology and load

Fig. 3 shows the SEM images of the Cu/AC and Zn salt-poisoned catalysts. As can be seen from Fig. 3(a) and (b), the Cu/AC catalyst has a good pore structure, and metal oxide particles of different sizes are distributed on the catalyst surface. After magnification by 5000 times (Fig. 3(b)), the pore structure, which is beneficial for the adsorption of the reaction gas, is still clearly visible. Fig. 3(c)–(e) show that most of the surface wall of the $ZnCl_2$–Cu/AC catalyst collapses, and the pore structure is seriously damaged, indicating that the AC structural strength
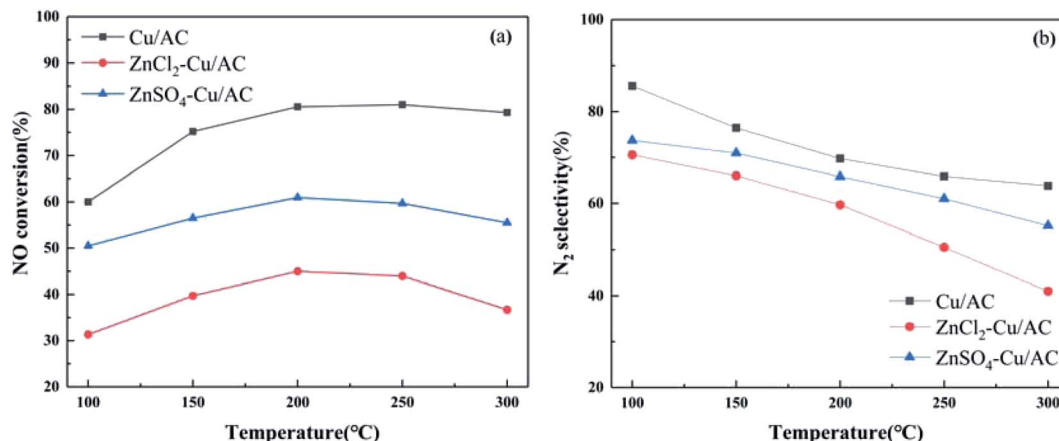
Fig. 2 CO-SCR performance of Cu/AC and Zn salt-poisoned catalysts at different temperatures: (a) NO conversion, and (b) N_2 selectivity.

decreases after $ZnCl_2$ doping. Fig. 3(f)–(h) shows that the $ZnSO_4$–Cu/AC catalyst matrix is damaged to a certain extent, the surface is rough, the pore structure is almost invisible, and only

large metal oxide particles are attached at certain positions, with local accumulation. This agglomeration phenomenon occurs on the catalyst surface after $ZnSO_4$ doping, which is not
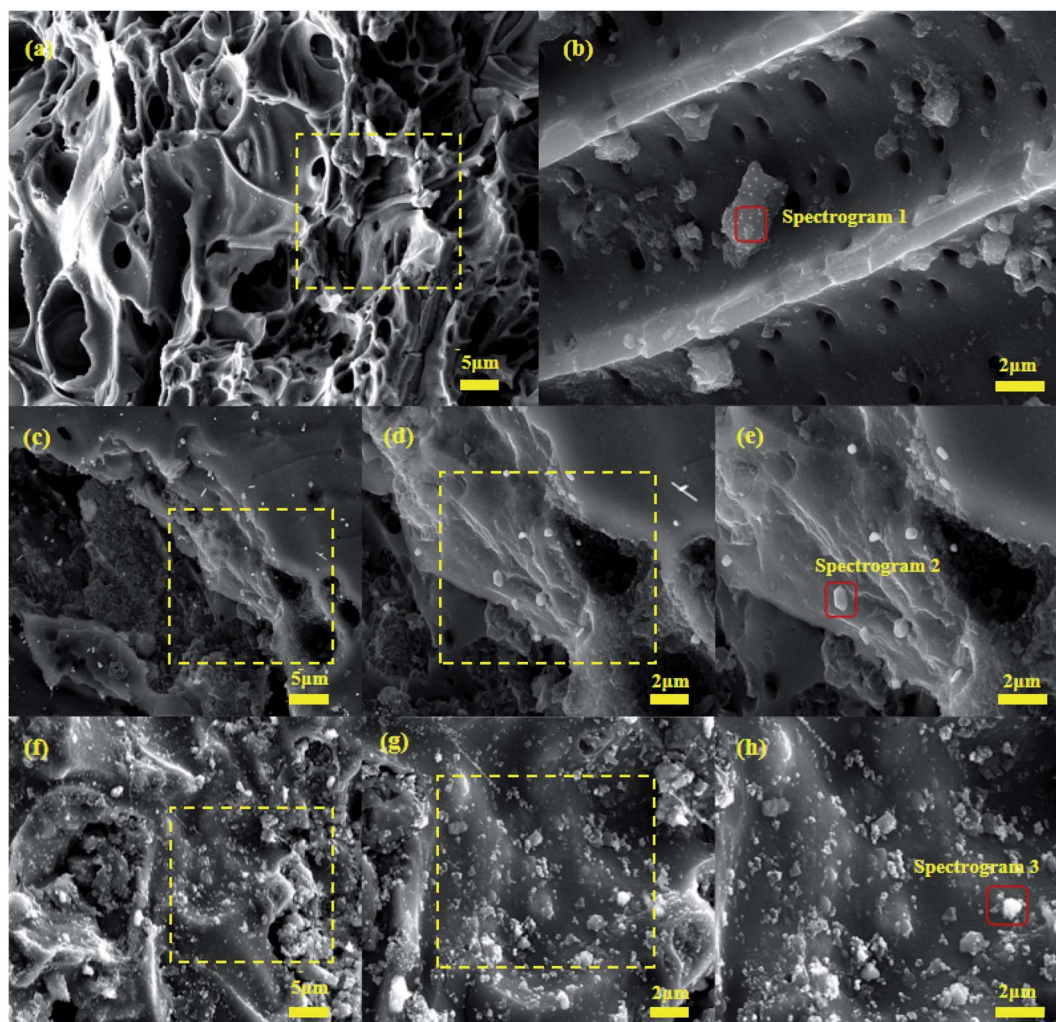

Fig. 3 SEM of Cu/AC and Zn salt-poisoned catalysts: (a) Cu/AC × 1500, (b) Cu/AC × 5000, (c) $ZnCl_2$−Cu/AC × 1500, (d) $ZnCl_2$−Cu/AC × 3500, (e) $ZnCl_2$−Cu/AC × 5000, (f) $ZnSO_4$−Cu/AC × 1500, (g) $ZnSO_4$−Cu/AC × 3500, and (h) $ZnSO_4$−Cu/AC × 5000.

conducive to the adsorption of CO and NO gas, leading to a decrease in the denitration activity.[27]

Next, the elemental composition of the catalysts was investigated *via* EDS characterization. The results are shown in Fig. 4, in which the EDS spectra (a), (b), and (c) correspond to Cu/AC surface spectrogram 1, $ZnCl_2$–Cu/AC surface spectrogram 2, and $ZnSO_4$–Cu/AC surface spectrogram 3, respectively. The obtained elements and their contents are summarized in Table 2, which shows that the surface of the three catalysts contains Cu, 9.09%, 14.58%, and 9.87%, respectively, confirming the successful loading of the active component Cu. Similarly, Zn was successfully loaded on the surface of the $ZnCl_2$- and $ZnSO_4$-doped catalysts at an amount of 3.53% and 4.37%, respectively, and the pores on the catalyst surface were clearly observed by SEM after doping the Zn salt. According to the denitration curve in Fig. 2(a), the denitration activity decreased significantly, inferring that zinc salt affected the denitration activity of the catalyst by reducing the adsorption performance of the catalyst.

3.3 Pore structure

Table 3 shows the BET characterization results of the Cu/AC and Zn salt-poisoned catalysts. The specific surface area of the Cu/

Table 2 Elemental content on the surface of the Cu/AC and Zn salt-poisoned catalysts

Spectrogram	Elements (%)			
	C	O	Cu	Zn
Spectrogram 1	83.69	7.21	9.09	—
Spectrogram 2	69.82	12.07	14.58	3.53
Spectrogram 3	53.45	32.32	9.87	4.37

AC catalyst is 631 m^2 g^{-1}, whereas that of $ZnCl_2$ and $ZnSO_4$ decreases to 538 and 600 m^2 g^{-1}, respectively. The specific surface area and pore structure of the catalyst affected the SCR denitrification activity to a certain extent, which was consistent with the denitrification activity shown in Fig. 2. This result is consistent with the denitration activity shown in Fig. 2. Fig. 5(a) shows that the relative pressures of the adsorption–desorption curves of the Cu/AC and Zn salt-poisoned catalysts are between 0.4 and 0.8. According to the IUPAC, all samples exhibited typical type IV adsorption isotherms and type H4 hysteresis rings,[32] which are consistent with a narrow aperture and stem from the layered structure. The results suggest the presence of a large number of micropores and mesopores in the catalyst,
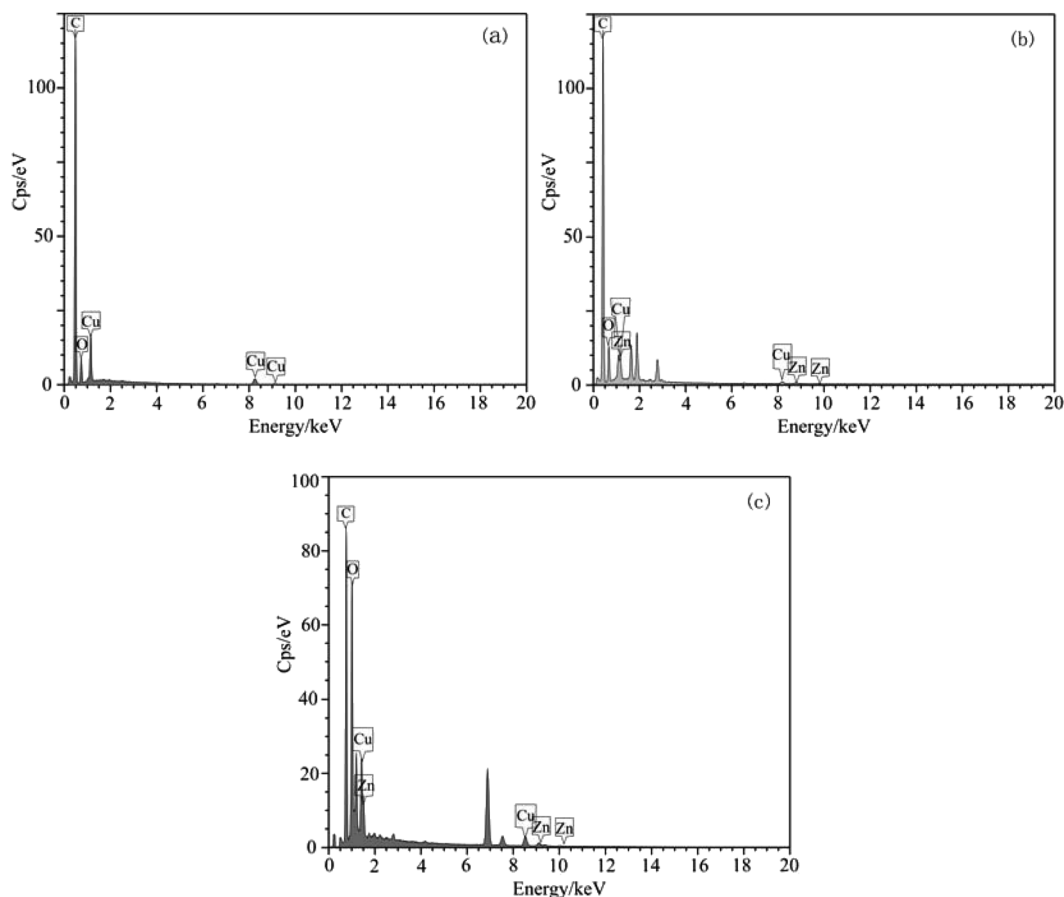

Fig. 4 Energy dispersive spectra of Cu/AC and Zn salt-poisoned catalysts: (a) Cu/AC spectrogram 1, (b) $ZnCl_2$–Cu/AC spectrogram 2, and (c) $ZnSO_4$–Cu/AC spectrogram 3.

Table 3 Pore parameters of different catalysts

Catalysts	Surface area ($m^2\ g^{-1}$)	Total pore volume ($cm^3\ g^{-1}$)	Average pore diameter (nm)
Cu/AC	631	0.31	1.96
ZnCl$_2$–Cu/AC	538	0.27	1.95
ZnSO$_4$–Cu/AC	600	0.30	1.90

but the total pore volume and average pore size decrease after Zn doping. Fig. 5(b) shows the average pore size distribution of the catalysts. The corresponding pore size distribution curve was determined according to the BJH method using the adsorption branch of the isotherm. The average pore size of Cu/AC, ZnCl$_2$–Cu/AC, and ZnSO$_4$–Cu/AC is 1.96, 1.95, and 1.90 nm, respectively. The specific surface area, total pore volume, and average pore size decreased slightly after doping zinc salt, which can be mainly attributed to the Zn salt particles covering the catalyst surface, blocking the pores, and reducing the contact area between the catalyst and the adsorbed gas.[30,31] In addition, the total pore volume decreases the most for the ZnCl$_2$-doped catalyst, which may be caused by the collapse of the catalyst surface. The average pore diameter of the ZnSO$_4$–Cu/AC catalyst is the smallest, mainly due to the blockage of the catalyst pore structure by metal particles. Nevertheless, the total pore volume is large, most likely because SO$_4{}^{2-}$ generates new pores and removes ash from the original pores during the poisoning process,[33] which is consistent with the SEM results. The decrease in the specific surface area and the average pore size of the catalyst is not conducive to the gas mass transfer, adsorption, and activation during the reaction process, resulting in the deactivation of the catalyst.[34]

3.4 Phase structure

Fig. 6 shows the XRD patterns of the Cu/AC and Zn salt-poisoned catalysts. The diffraction peak observed at 20°–30° can be attributed to the (002) crystal plane of graphite microcrystals with a layered structure (JCPSF 13-0148).[35] The peak decreases after ZnCl$_2$ doping and decreases and becomes

sharper after ZnSO$_4$ doping. In addition, diffraction peaks corresponding to (111), (220), and (211) CuO crystal planes (PDF no. 65-3288) can be observed at 2θ values of 36.266°, 42.820°, and 61.380° for the Cu/AC and Zn salt-poisoned catalysts.[36] Diffraction peaks corresponding to (111), (200), and (211) Cu$_2$O crystal planes are observed at 2θ values of 40.491°, 50.439°, and 74.121° (PDF no. 65-2309). The absence of ZnO diffraction peaks in the XRD patterns of the Cu/AC and Zn salt-poisoned catalysts indicates that the primary crystals formed by Zn oxide are smaller than 4 nm and mainly distributed on the surface of the catalyst in a highly dispersed or amorphous form.[37] Only two characteristic diffraction peaks attributable to Cu species are observed on the catalyst surface, indicating that the active metals are mainly in the form of Cu$_2$O and CuO. The crystallization performance of the Cu/AC catalyst at all angles is very good and not sharp, indicating that the Cu oxide supported on AC is evenly dispersed. The characteristic diffraction peaks of the monoclinic crystal phase appear at 42.820°, 50.439°, and 74.121°, suggesting that CuO and Cu$_2$O exhibit high crystallinity, relatively large grains, and agglomeration, which is in accord with the SEM and EDS results and confirms that the addition of Zn inhibits the dispersion of CuO and Cu$_2$O and decreases the denitration activity of the catalyst. In addition, the XRD pattern of the ZnCl$_2$–Cu/AC catalyst shows sharper diffraction peaks than that of the ZnSO$_4$–Cu/AC catalyst and the agglomeration phenomenon is more evident, which is consistent with the results of the denitration curve and can explain the more serious toxicity of ZnCl$_2$.

3.5 Valence state of the element

The active component valence and element concentration of the catalysts were studied by XPS, and the results are shown in Table 4. Fig. 7(a) shows the O 1s XPS spectra of the Cu/AC and Zn salt-poisoned catalysts. The fitted peaks can be assigned to the three types of oxygen atoms: lattice oxygen O$_\alpha$ (approx. 529.0–530.0 eV), chemisorbed oxygen O$_\beta$ (approx. 531.3–531.9 eV), and hydroxyl O$_\gamma$ (approx. 532.7–533.5 eV).[38] As can be extracted from Table 4 and Fig. 7(a), Zn doping leads to
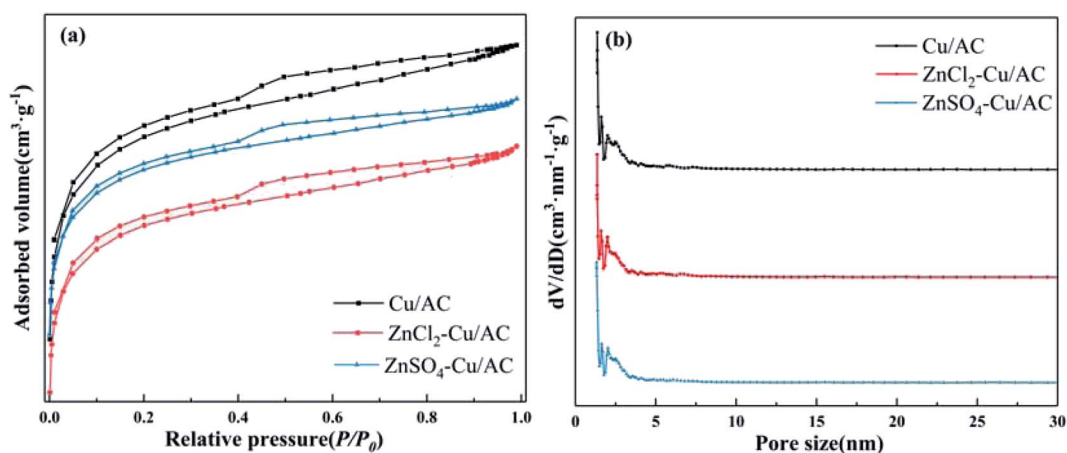

Fig. 5 Pore characterization of Cu/AC and Zn salt-poisoned catalysts: (a) N$_2$ adsorption–desorption, and (b) pore diameter distribution.
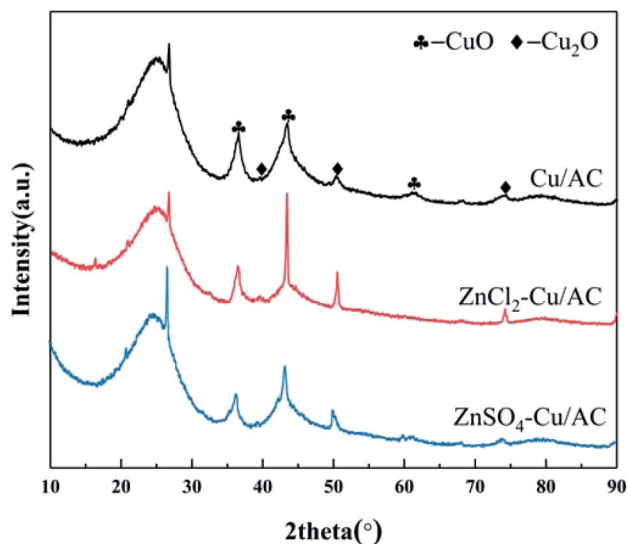
Fig. 6 XRD patterns of Cu/AC and Zn salt-poisoned catalysts.

a significant decrease in the content of O_β in the order Cu/AC > $ZnSO_4$–Cu/AC > $ZnCl_2$–Cu/AC. Studies have shown that O_β is the most mobile reactive oxygen species in SCR.[39] In addition, a higher percentage of O_β contributes to the oxidation of NO to NO_2, and the SCR activity is enhanced by a "rapid SCR" reaction ($CO + NO + NO_2 \rightarrow 2N_2 + 2CO_2$). As shown in Table 4, the concentration of O_β decreases significantly after Zn doping, indicating that the Zn salt can inhibit the formation of O_β, which reduces the denitration efficiency of the catalyst. After $ZnCl_2$ doping, the concentration of O_β is lower than that of the $ZnSO_4$-doped catalyst, which is detrimental to the SCR denitration reaction and in accord with the results of the CO-SCR denitration activity.

Fig. 7(b) shows the XPS spectra of the Cu/AC and Zn salt-poisoned catalysts. The peaks at binding energies of ∼933.2 and ∼953.1 eV correspond to Cu $2p_{3/2}$ and Cu $2p_{1/2}$ of Cu^0, respectively. The energy difference between the two spin states is 19.9 eV due to spin–orbit coupling. Meanwhile, the peaks at ∼934.2 and ∼954.2 eV correspond to Cu $2p_{3/2}$ and Cu $2p_{1/2}$ of Cu^{2+}, respectively,[40] and those at ∼932.1 and ∼951.5 eV can be attributed to Cu $2p_{3/2}$ and Cu $2p_{1/2}$ of Cu^+, respectively.[41] Most of the NO adsorbed on Cu^{2+} can be quickly converted to N_2, and Cu^{2+} has a good catalytic effect on the removal of NO; therefore, the high catalytic activity of Cu^{2+} is conducive to the adsorption and activation of NO and CO. Fig. 7(b) shows that after $ZnCl_2$ and $ZnSO_4$ doping, the Cu^{2+} content on the surface of the Cu/AC catalyst decreases from 44.37% to 15.95% and 23.42%,

respectively, indicating that the Zn salt doping decreases the proportion of Cu^{2+}, thus reducing the denitration capacity.[42] In addition, the Cu^{2+} content on the $ZnCl_2$–Cu/AC catalyst exhibits the lowest Cu^{2+} content and the highest toxicity.[43] According to previous studies, SO_4^{2-} ions can promote the continuous replenishment of O_β,[31] which is in agreement with the lower toxicity of the $ZnSO_4$–doped catalyst compared with the $ZnCl_2$–Cu/AC catalyst.

Fig. 7(c) shows the spectra of Zn 2p XPS spectra as a Zn salt-poisoned catalysts. The peaks at ∼1022.2 and ∼1045.3 eV correspond to Zn $2p_{3/2}$ and Zn $2p_{1/2}$, respectively,[30] indicating that Zn is in the divalent state in the Zn salt-poisoned catalysts. It is clear from the figure that the Zn^{2+} content is lower in $ZnCl_2$–Cu/AC than in $ZnSO_4$–Cu/AC. This is consistent with the EDS result, suggesting that Zn^{2+} occupies the active site and oxygen vacancies,[42] thus affecting the denitration activity.

3.6 Surface functional groups

Fig. 8 shows the FTIR spectra of the Cu/AC and Zn salt-poisoned catalysts. The absorption peak at 3414 cm^{-1} is generally attributed to the stretching vibration of carboxyl and O–H functional groups.[44,45] The peak at 1618 cm^{-1} is due to the C=O stretching vibration of the aliphatic group.[46] The absorption peak at 1390 cm^{-1} is ascribable to the C–H stretching vibration of naphthenes and aliphatic hydrocarbons.[46] The absorption peak at 1128 cm^{-1} is due to the C–O stretching vibration of the C–O–C bonds of functional groups such as lactone, phenol, and ether on the AC surface.[46,47] The stretching vibration peaks of the carboxyl and O–H groups at 3412 cm^{-1} weaken after the Zn salt doping, which may be caused by substituting H atoms of the –OH group by Zn resulting in a decrease in the number of active sites for the adsorption reaction.[31] Furthermore, the peak corresponding to the asymmetric vibration of the lactone group at 1621 and 1625 cm^{-1} weakens significantly. Teng *et al.*[48] found that NO adsorption occurs in the C=O moiety and surface oxygen functional groups can improve the dispersion of active components and form CO adsorption sites, whereas Zn^{2+} decreases the number of C=O groups. The intensity of the C–O stretching vibration peak at 1138 and 1140 cm^{-1} decreases, which might be due to the occupation of oxygen vacancies or active sites.[28] In summary, the catalyst deactivation after Zn salt doping is attributed to the occupation of oxygen vacancies by Zn^{2+} that reduces the number of oxygen-containing functional groups such as carboxyl and lactone groups, which in turn decreases the surface acidity and active sites. Simultaneously, the introduced Zn interacts strongly with Cu species, disrupting the Cu–O–H and Cu–C=O structures.[49] Moreover, Cl$^-$ occupies the surface active sites of the catalyst, severely inhibiting the fluidity of O_β and enhancing the toxicity, which is consistent with the XPS results. Additionally, SO_4^{2+} increases the Brønsted acidity in the catalyst surface and offsets the destruction of oxygen-containing functional groups by Zn^{2+}.[49] Therefore, the denitrification rate of $ZnCl_2$–Cu/AC is lower than that of $ZnSO_4$–Cu/AC, and the gap becomes larger with the increase in temperature, which may be one of the reasons for the higher toxicity of $ZnCl_2$ than $ZnSO_4$.

Table 4 Surface atomic concentration of different catalyst samples

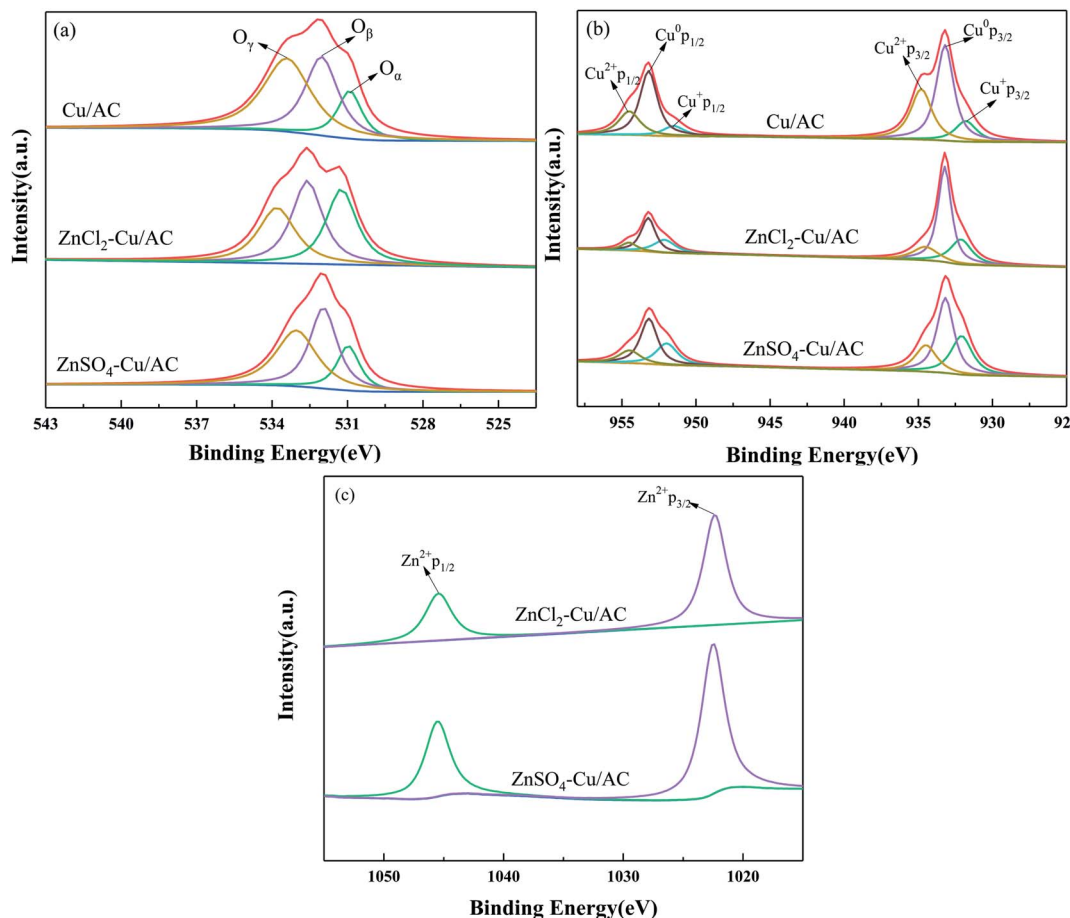| Catalysts	$O_\beta/(O_\alpha + O_\beta + O_\gamma)$%	$Cu^{2+}/(Cu^0 + Cu^+ + Cu^{2+})$%	$Cu^+/(Cu^0 + Cu^+ + Cu^{2+})$%
Cu/AC	50.20	44.37	19.33
$ZnCl_2$–Cu/AC	34.96	15.95	24.25
$ZnSO_4$–Cu/AC	43.62	23.42	38.07

Fig. 7 XPS of Cu/AC and Zn salts-poisoned catalysts: (a) O 1s, (b) Cu 2p, and (c) Zn 2p.

3.7 Mechanism of catalytic denitration

The low-temperature denitration *via* CO-SCR reaction over the Cu/AC catalyst surface is a representative heterogeneous catalytic system that follows the Langmuir–Hinshelwood reaction mechanism.[50] Accordingly, the denitration mechanism

Fig. 8 Fourier transform infrared spectrum of Cu/AC and Zn salts-poisoned catalysts.

depicted in Fig. 9 for the CO reduction of NO over the Cu/AC catalyst was proposed. The active component Cu is uniformly dispersed on the AC, which increases the specific surface area of the catalyst, as shown in Table 4, and enhances the adsorption of NO and CO. This conclusion indicates that Cu is uniformly distributed on the surface of the Cu/AC catalyst in Fig. 2, which improves the denitration efficiency up to 80%. CO is adsorbed on the catalyst surface to reduce $-O-Cu^{2+}$ to $=Cu^{\delta+}$ and generate CO_2 (eqn (6)–(8)). The adsorbed NO dissociates into N and O, and the dissociated N atom combines with an NO molecule to form N_2O (eqn (9)–(11)).[51] It has been reported that the dissociation of NO is a key step for the CO-induced elimination of NO.[52] The release of the active sites promotes the adsorption of CO, and finally, N_2O and $=Cu^{\delta+}$ react to generate N_2 and $-O-Cu^{2+}$ (eqn (12)), which further promotes the denitration reaction. In the reaction of CO with NO, the $Cu^{2+} \leftrightarrow Cu^{\delta+}$ exchange may alter the valence state of the catalyst surface, and more oxygen vacancies may be available for the conversion process, promoting the conversion of NO to N_2. This is consistent with Pan's proposal of the Mars–van Krevelen mechanism (redox process).[53]
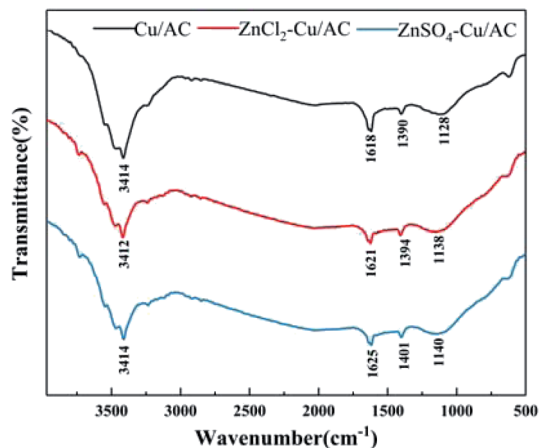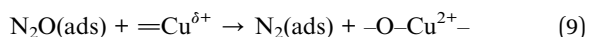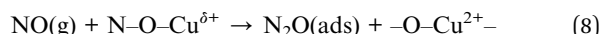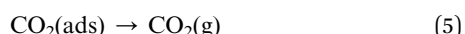
$$CO(g) \rightarrow CO(ads) \tag{3}$$

Fig. 9 Mechanisms of the CO reduction of NO.

$$-O-Cu^{2+}- + CO(ads) \rightarrow =Cu^{\delta+} + CO_2(ads) \quad (4)$$

$$CO_2(ads) \rightarrow CO_2(g) \quad (5)$$

$$NO(g) \rightarrow NO(ads) \quad (6)$$

$$NO(ads) + =Cu^{\delta+} \rightarrow N-O-Cu^{\delta+} \quad (7)$$

$$NO(g) + N-O-Cu^{\delta+} \rightarrow N_2O(ads) + -O-Cu^{2+}- \quad (8)$$

$$N_2O(ads) + =Cu^{\delta+} \rightarrow N_2(ads) + -O-Cu^{2+}- \quad (9)$$
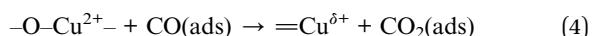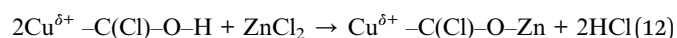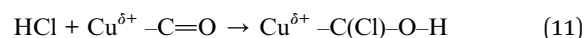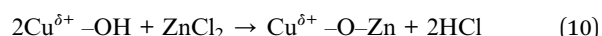
3.8 Mechanism of Zn salt poisoning on the Cu/AC catalyst

On the basis of clarifying the denitrification mechanism, the toxicity mechanism of Zn salt on Cu/AC catalyst was further studied. According to the results presented in Table 2 and Fig. 3, the Cu/AC catalyst has a good pore structure with the active component Cu evenly dispersed on the surface of the catalyst, which is advantageous for the adsorption and loading of the reactive gas. However, the Zn salt doping on the surface of the catalyst destroys the pore structure of the catalyst. As can be extracted from Table 3 and Fig. 5, the specific surface area, total pore volume, and average pore size of the Zn salt-poisoned catalyst decrease, thus significantly reducing the physical adsorption capacity for CO and NO. Fig. 6 shows that with the Zn salt doping, the crystallization and agglomeration of CuO and Cu_2O appear on the catalyst surface, not only blocking the pores and occupying the active site but also hindering the participation of some active components in the denitration reaction. As can be seen from Table 4 and Fig. 7, the content of effective active component Cu^{2+} on the surface of the catalyst doped with Zn salt decreases, resulting in a decrease in oxygen vacancies and O_β, in the interaction with CO and NO, in the rapid SCR (eqn (5)–(9)), and in the concentration of intermediate N_2O. This inevitably reduces the denitration efficiency of

the catalyst.[53] $ZnCl_2$ occupies the oxygen vacancies and active sites and reacts with –OH and C=O to reduce the oxygen-containing functional groups and the surface acidity of the catalyst (Fig. 8). Cl^- not only occupies the oxygen vacancies but also inhibits the fluidity of O_β and enhances the toxicity. The BET results show that the specific surface area of the catalyst is significantly reduced after $ZnCl_2$ doping. In the $ZnSO_4$–Cu/AC catalyst, new pores are generated by the reaction with SO_4^{2-} and the ash content of the original pores is removed. The average pore size decreases, but the specific surface area and total pore volume increase compared with those of $ZnCl_2$–Cu/AC. The results of the N_2 selectivity and XPS analysis show that $ZnSO_4$ occupies the oxygen vacancies but increases the surface acidity and promotes the supplement of O_β, thus alleviating the toxicity of the catalyst. As a result, $ZnCl_2$ is more toxic than $ZnSO_4$. On the basis of the above characterization results and the denitration mechanism, the mechanism shown in Fig. 10 was proposed to explain the toxicity of $ZnCl_2$ and $ZnSO_4$ on the Cu/AC catalyst.

On the basis of the aforementioned characterization and analysis results, the following toxicological mechanisms of zinc salts on Cu/AC catalysts were proposed: $ZnCl_2$ interacts with $Cu^{\delta+}$–OH to form a $Cu^{\delta+}$–O–Zn complex and H^+ and Cl^- react to form HCl (eqn (10)), which then reacts with $Cu^{\delta+}$–C=O to form $Cu^{\delta+}$–C(Cl)–O–H (eqn (11)). Finally, $Cu^{\delta+}$–C(Cl)–O–H and $ZnCl_2$ produce a $Cu^{\delta+}$–C(Cl)–O–Zn complex (eqn (12)). Similarly, $ZnSO_4$ and $Cu^{\delta+}$–OH form a $Cu^{\delta+}$–O–Zn complex and H_2SO_4 (eqn (13)), and $ZnSO_4$ and $Cu^{\delta+}$–C(Cl)–O–H form a $Cu^{\delta+}$–C–O–Zn complex (eqn (14)).

$$2Cu^{\delta+} -OH + ZnCl_2 \rightarrow Cu^{\delta+} -O-Zn + 2HCl \quad (10)$$

$$HCl + Cu^{\delta+} -C=O \rightarrow Cu^{\delta+} -C(Cl)-O-H \quad (11)$$

$$2Cu^{\delta+} -C(Cl)-O-H + ZnCl_2 \rightarrow Cu^{\delta+} -C(Cl)-O-Zn + 2HCl \quad (12)$$
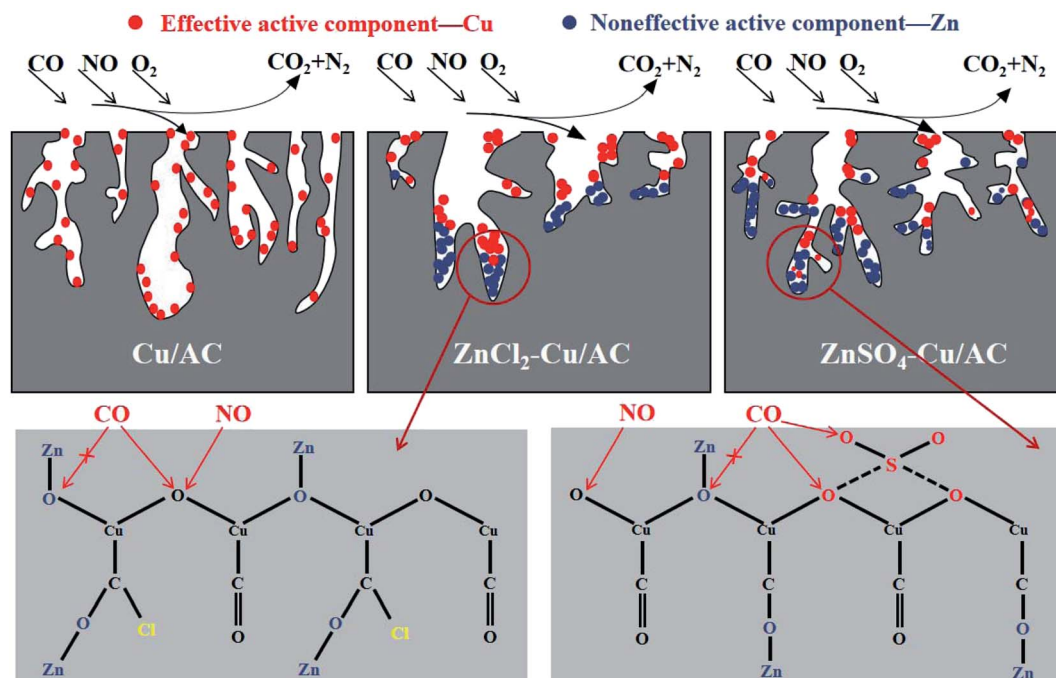
Fig. 10 Toxicity mechanism of Cu/AC catalysts poisoned by ZnCl$_2$ and ZnSO$_4$.

$$2Cu^{\delta+} - O - H + ZnSO_4 \rightarrow Cu^{\delta+} - O - Zn + 2H_2SO_4 \tag{13}$$

$$Cu^{\delta+} - C = O + ZnSO_4 \rightarrow Cu^{\delta+} - C - O - Zn + 2H_2SO_4 \tag{14}$$
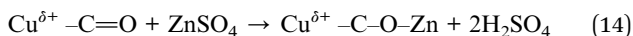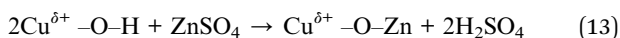
In conclusion, Zn^{2+} occupies the oxygen vacancies on the surface of the catalyst, which inhibits the adsorption of CO and NO. Meanwhile, the dissociation of NO is inhibited and the intermediate N$_2$O decreases, resulting in the reduction of active sites and inhibition of the adsorption of CO. The Cu–O–H and Cu–C=O structures are destroyed by Zn salts, and the number of oxygen-containing functional groups, such as carboxyl and lactone, decreases, thereby decreasing surface acidity and active sites. It is worth noting that the presence of Cl$^-$ can severely inhibit the O$_\beta$ mobility, resulting in serious toxicity.

4 Conclusions

The mechanism of zinc salt on Cu/AC catalyst CO-SCR denitrification at low temperatures was discussed as follows. Zn^{2+} competes with CO and NO for the active sites for CO adsorption, which reduces the physical adsorption capacity for CO and NO. The agglomeration of CuO and Cu$_2$O on the catalyst surface and the blockage of the pores by Zn particles damage the pore structure and decrease the specific surface area. Due to the interaction between Zn and Cu oxides, Zn^{2+} reacts with Cu–O–H and Cu–C=O, resulting in the reduction of oxygen-containing functional groups and the active sites and oxygen vacancies. The Zn doping decreases the concentration of Cu^{2+} and O$_\beta$ and inhibits the denitration reaction. In addition, the toxicity of ZnCl$_2$ is more serious than that of ZnSO$_4$ because Cl$^-$ not only occupies oxygen vacancies but also inhibits the O$_\beta$ migration. In contrast, SO$_4^{2-}$ increases the surface acidity and promotes the

O$_\beta$ supplementation. In conclusion, in addition to the reduction of the specific surface area, the decrease in the amount of Cu^{2+} and O$_\beta$ is the main reason for the deactivation of the CO-SCR catalyst at low temperatures.

Conflicts of interest

There are no conflicts to declare.

Acknowledgements

References

1 R. T. Guo, W. G. Pan, J. X. Ren, X. B. Zhang and Q. Jin, Absorption of NO from simulated flue gas by using NaClO$_2$/(NH$_4$)(2)CO$_3$ solutions in a stirred tank reactor, *Korean J. Chem. Eng.*, 2013, **30**(1), 101–104.

2 M. Y. Jiang, K. Yang, H. J. Yu and L. Yao, Density functional theory of transition metal oxide (FeO, CuO and MnO) adsorbed on TiO$_2$ surface, *J. Phys. Chem. Solids*, 2021, **152**, 109957.

3 X. Wu, Y. Feng, Y. Du, X. Liu, C. Zou and Z. Li, Enhancing DeNO$_x$ performance of CoMnAl mixed metal oxides in low-temperature NH$_3$-SCR by optimizing layered double hydroxides (LDHs) precursor template, *Appl. Surf. Sci.*, 2019, **467**, 802–810.

4 B.-T. Liu, C.-J. Huang, Y.-X. Ke, W.-H. Wang, H.-L. Kuo, D. Lin, V. Lin and S.-H. Lin, Enhanced selective catalytic reduction of NO over Mn-Ce catalysts with the acetic-acid-chelated titania support at low temperature, *Appl. Catal., A*, 2017, **538**, 74–80.

5 J. Liu, G.-q. Li, Y.-f. Zhang, X.-q. Liu, Y. Wang and Y. Li, Novel Ce-W-Sb mixed oxide catalyst for selective catalytic reduction of NO_x with NH_3, *Appl. Surf. Sci.*, 2017, **401**, 7–16.

6 T. Liu, J. Qian, Y. Yao, Z. Shi, L. Han, C. Liang, B. Li, L. Dong, M. Fan and L. Zhang, Research on SCR of NO with CO over the $Cu_{0.1}La_{0.1}Ce_{0.8}O$ mixed-oxide catalysts: effect of the grinding, *Mol. Catal.*, 2017, **430**, 43–53.

7 A. Patel, P. Shukla, J. Chen, T. E. Rufford, S. Wang, V. Rudolph and Z. Zhu, Structural sensitivity of mesoporous alumina for copper catalyst loading used for NO reduction in presence of CO, *Chem. Eng. Res. Des.*, 2015, **101**, 27–43.

8 L. F. Oton, A. C. Oliveira, J. C. S. de Araujo, R. S. Araujo, F. F. de Sousa, G. D. Saraiva, R. Lang, L. Otubo, G. C. da Silva Duarte and A. Campos, Selective catalytic reduction of NO_x by CO (CO-SCR) over metal-supported nanoparticles dispersed on porous alumina, *Adv. Powder Technol.*, 2020, **31**(1), 464–476.

9 L. Zhang, Y.-h. Qin, B.-z. Chen, Y.-g. Peng, H.-b. He and Y. Yuan, Catalytic reduction of SO_2 by CO over CeO_2-TiO_2 mixed oxides, *Trans. Nonferrous Met. Soc. China*, 2016, **26**(11), 2960–2965.

10 G. Carollo, A. Garbujo, Q. Xin, J. Fabro, P. Cool, P. Canu and A. Glisenti, $CuO/La_{0.5}Sr_{0.5}CoO_3$ nanocomposites in TWC, *Appl. Catal., B*, 2019, **255**, 117753.

11 X. Dai, W. Jiang, W. Wang, X. Weng, Y. Shang, Y. Xue and Z. Wu, Supercritical water syntheses of transition metal-doped CeO_2 nano-catalysts for selective catalytic reduction of NO by CO: an in situ diffuse reflectance Fourier transform infrared spectroscopy study, *Chin. J. Catal.*, 2018, **39**(4), 728–735.

12 Q. Guo, W. Jing, Y. Hou, Z. Huang, G. Ma, X. Han and D. Sun, On the nature of oxygen groups for NH_3-SCR of NO over carbon at low temperatures, *Chem. Eng. J.*, 2015, **270**, 41–49.

13 K. Huang, L. Lin, K. Yang, W. Dai, X. Chen and X. Fu, Promotion effect of ultraviolet light on NO plus CO reaction over Pt/TiO_2 and Pt/CeO_2-TiO_2 catalysts, *Appl. Catal., B*, 2015, **179**, 395–406.

14 J. Ohyama, J. Shibano, A. Satsuma, R. Fukuda, Y. Yamamoto, S. Arai, T. Shishido, H. Asakura, S. Hosokawa and T. Tanaka, Quantum Chemical Computation-Driven Development of Cu-Shell-Ru-Core Nanoparticle Catalyst for NO Reduction Reaction, *J. Phys. Chem. C*, 2019, **123**(33), 20251–20256.

15 G. Cheng, X. Tan, X. Song, X. Chen, W. Dai, R. Yuan and X. Fu, Visible light assisted thermocatalytic reaction of CO plus NO over $Pd/LaFeO_3$, *Appl. Catal., B*, 2019, **251**, 130–142.

16 K. Ueda, M. Tsuji, J. Ohyama and A. Satsuma, Tandem Base-Metal Oxide Catalyst: Superior NO Reduction Performance to the Rh Catalyst in NO-C_3H_6-CO-O_2, *ACS Catal.*, 2019, **9**(4), 2866–2869.

17 X. Wang, X. Wu, N. Maeda and A. Baiker, Striking activity enhancement of gold supported on Al-Ti mixed oxide by promotion with ceria in the reduction of NO with CO, *Appl. Catal., B*, 2017, **209**, 62–68.

18 L. Zhang, L. Huang, Y.-h. Qin and B.-z. Chen, Structure and denitration performance of carbon-based catalysts prepared from Cu-BTC precursor, *Trans. Nonferrous Met. Soc. China*, 2018, **28**(5), 980–988.

19 J.-c. Wang, Y. Chen, L. Tang, W.-r. Bao, L.-p. Chang and L.-n. Han, One-step hydrothermal synthesis of Cu-SAPO-34/cordierite and its catalytic performance on NO_x removal from diesel vehicles, *Trans. Nonferrous Met. Soc. China*, 2013, **23**(11), 3330–3336.

20 S. Guerrero, I. Guzman, G. Aguila, B. Chornik and P. Araya, Study of $Na/Cu/TiO_2$ catalysts for the storage and reduction of NO, *Appl. Catal., B*, 2012, **123**, 282–295.

21 S. Guerrero, I. Guzman, G. Aguila and P. Araya, Sodium-promoted NO adsorption under lean conditions over Cu/TiO_2 catalysts, *Catal. Commun.*, 2009, **11**(1), 38–42.

22 F. Lin, X. Wu and D. Weng, Effect of barium loading on CuO_x-CeO_2 catalysts: NO_x storage capacity, NO oxidation ability and soot oxidation activity, *Catal. Today*, 2011, **175**(1), 124–132.

23 D. Wang, B. Huang, Z. Shi, H. Long, L. Li, Z. Yang and M. Dai, Influence of cerium doping on Cu-Ni/activated carbon low-temperature CO-SCR denitration catalysts, *RSC Adv.*, 2021, **11**(30), 18458–18467.

24 C. Liu, J.-W. Shi, C. Gao and C. Niu, Manganese oxide-based catalysts for low-temperature selective catalytic reduction of NO_x with NH_3: a review, *Appl. Catal., A*, 2016, **522**, 54–69.

25 J. Li, Y. Peng, H. Chang, X. Li, J. C. Crittenden and J. Hao, Chemical poison and regeneration of SCR catalysts for NO_x removal from stationary sources, *Front. Environ. Sci. Eng.*, 2016, **10**(3), 413–427.

26 X. Wu, Z. Si, G. Li, D. Weng and Z. Ma, Effects of cerium and vanadium on the activity and selectivity of MnO_x-TiO_2 catalyst for low-temperature NH_3-SCR, *J. Rare Earths*, 2011, **29**(1), 64–68.

27 L. Qi, J. Li, Y. Yao and Y. Zhang, Heavy metal poisoned and regeneration of selective catalytic reduction catalysts, *J. Hazard. Mater.*, 2019, **366**, 492–500.

28 Z.-h. Su, S. Ren, T.-s. Zhang, J. Yang, Y.-h. Zhou and L. Yao, Effects of PbO poisoning on Ce-Mn/AC catalyst for low-temperature selective catalytic reduction of NO with NH_3, *J. Iron Steel Res. Int.*, 2021, **28**(2), 133–139.

29 Z. Ali, Y.-w. Wu, Y. Wu, Z. Arain, M.-x. Xu, Q. Lu, H. Ma and H.-y. Zhao, Inhibition effects of Pb species on the V_2O_5-MoO_3/TiO_2 catalyst for selective catalytic reduction of NO_x with NH_3: a DFT supported experimental study, *Appl. Surf. Sci.*, 2020, **525**, 146582.

30 R.-t. Guo, Q.-s. Wang, W.-g. Pan, Q.-l. Chen, H.-l. Ding, X.-f. Yin, N.-z. Yang, C.-z. Lu, S.-x. Wang and Y.-c. Yuan, The poisoning effect of heavy metals doping on Mn/TiO_2 catalyst for selective catalytic reduction of NO with NH_3, *J. Mol. Catal. A: Chem.*, 2015, **407**, 1–7.

31 Z. Su, S. Ren, J. Yang, L. Yao, Y. Zhou, Z. Chen and T. Zhang, Poisoning Effect Comparison of ZnCl(2)and ZnSO(4)on Mn-Ce/AC Catalyst for Low-Temperature SCR of NO, *ChemistrySelect*, 2020, **5**(29), 9226–9234.

32 L. J. Jiang, Q. C. Liu, Q. Zhao, S. Ren, M. Kong, L. Yao and F. Meng, Promotional effect of Ce on the SCR of NO with NH_3 at low temperature over $MnO(x)$ supported by nitric acid-modified activated carbon, *Res. Chem. Intermed.*, 2018, **44**(3), 1729–1744.

33 Z. Yan, H. Yang, J. Ouyang and A. Tang, In situ loading of highly-dispersed CuO nanoparticles on hydroxyl-group-rich SiO_2-AlOOH composite nanosheets for CO catalytic oxidation, *Chem. Eng. J.*, 2017, **316**, 1035–1046.

34 C. Sun, Y. Tang, F. Gao, J. Sun, K. Ma, C. Tang and L. Dong, Effects of different manganese precursors as promoters on catalytic performance of CuO-MnO_x/TiO_2 catalysts for NO removal by CO, *Phys. Chem. Chem. Phys.*, 2015, **17**(24), 15996–16006.

35 L. Wang, X. Cheng, Z. Wang, C. Ma and Y. Qin, Investigation on Fe-Co binary metal oxides supported on activated semi-coke for NO reduction by CO, *Appl. Catal., B*, 2017, **201**, 636–651.

36 K. Malaie, M. R. Ganjali, T. Alizadeh and P. Norouzi, Simple electrochemical preparation of nanoflake-like copper oxide on Cu-plated nickel foam for supercapacitor electrodes with high areal capacitance, *J. Mater. Sci.: Mater. Electron.*, 2017, **28**(19), 14631–14637.

37 H. Li, R. Cheng, Z. Liu and C. Du, Waste control by waste: Fenton-like oxidation of phenol over Cu modified ZSM-5 from coal gangue, *Sci. Total Environ.*, 2019, **683**, 638–647.

38 W. T. Yao, S. H. Yu, S. Y. Zhou, J. Jiang, Q. S. Wu, L. Zhang and J. Jiang, Formation of uniform CuO nanorods by spontaneous aggregation: selective synthesis of CuO, Cu_2O, and Cu nanoparticles by a solid-liquid phase arc discharge process, *J. Phys. Chem. B*, 2005, **109**(29), 14011–14016.

39 F. D. Liu and H. He, Structure-Activity Relationship of Iron Titanate Catalysts in the Selective Catalytic Reduction of NO_x with NH_3, *J. Phys. Chem. C*, 2010, **114**(40), 16929–16936.

40 A. Sharma, R. K. Dutta, A. Roychowdhury, D. Das, A. Goyal and A. Kapoor, Cobalt doped CuO nanoparticles as a highly efficient heterogeneous catalyst for reduction of 4-nitrophenol to 4-aminophenol, *Appl. Catal., A*, 2017, **543**, 257–265.

41 L. Liu, X. Wu, Y. Ma, X. Zhang, R. Ran, Z. Si and D. Weng, Potassium deactivation of Cu-SSZ-13 catalyst for NH_3-SCR: evolution of salts, zeolite and copper species, *Chem. Eng. J.*, 2020, **383**, 123080.

42 Z. Xu, Y. Li, J. Guo, J. Xiong, Y. Lin and T. Zhu, An efficient and sulfur resistant K-modified activated carbon for SCR denitrification compared with acid- and Cu-modified activated carbon, *Chem. Eng. J.*, 2020, **395**, 125047.

43 Y. K. Yu, J. F. Miao, J. X. Wang, C. He and J. S. Chen, Facile synthesis of $CuSO_4/TiO_2$ catalysts with superior activity and SO_2 tolerance for NH_3-SCR: physicochemical properties and reaction mechanism, *Catal. Sci. Technol.*, 2017, **7**(7), 1590–1601.

44 J. M. Pena, N. S. Allen, M. Edge, C. M. Liauw, F. Santamaria, O. Noiset and B. Valange, Factors affecting the adsorption of stabilisers on to carbon black (flow micro-calorimetry and FTIR studies) – Part I – primary phenolic antioxidants, *J. Mater. Sci.*, 2001, **36**(12), 2885–2898.

45 J. Yu and J. So, Synthesis and characterization of nitrogen-containing hydrothermal carbon with ordered mesostructure, *Chem. Phys. Lett.*, 2019, **716**, 237–246.

46 Y. Cao, Y. Gu, K. Wang, X. Wang, Z. Gu, T. Ambrico, M. A. Castro, J. Lee, W. Gibbons and J. A. Rice, Adsorption of creatinine on active carbons with nitric acid hydrothermal modification, *J. Taiwan Inst. Chem. Eng.*, 2016, **66**, 347–356.

47 Y. Lin, Y. Li, Z. Xu, J. Xiong and T. Zhu, Transformation of functional groups in the reduction of NO with NH_3 over nitrogen-enriched activated carbons, *Fuel*, 2018, **223**, 312–323.

48 H. S. Teng, Y. T. Tu, Y. C. Lai and C. C. Lin, Reduction of NO with NH_3 over carbon catalysts – the effects of treating carbon with H_2SO_4 and HNO_3, *Carbon*, 2001, **39**(4), 575–582.

49 S. Ren, S. Li, Z. Su, J. Yang, H. Long, M. Kong, J. Yang and Z. Cai, Poisoning effects of KCl and As_2O_3 on selective catalytic reduction of NO with NH_3 over Mn-Ce/AC catalysts at low temperature, *Chem. Eng. J.*, 2018, **351**, 540–547.

50 Y. Zhang, L. Zhao, J. Duan and S. Bi, Insights into $deNO(x)$ processing over Ce-modified Cu-BTC catalysts for the CO-SCR reaction at low temperature by in situ DRIFTS, *Sep. Purif. Technol.*, 2020, **234**, 116081.

51 T. Liu, Y. Yao, L. Wei, Z. Shi, L. Han, H. Yuan, B. Li, L. Dong, F. Wang and C. Sun, Preparation and Evaluation of Copper Manganese Oxide as a High-Efficiency Catalyst for CO Oxidation and NO Reduction by CO, *J. Phys. Chem. C*, 2017, **121**(23), 12757–12770.

52 C. Deng, J. Qian, C. Yu, Y. Yi, P. Zhang, W. Li, L. Dong, B. Li and M. Fan, Influences of doping and thermal stability on the catalytic performance of $CuO/Ce_{20}M_1O_x$(M = Zr, Cr, Mn, Fe, Co, Sn) catalysts for NO reduction by CO, *RSC Adv.*, 2016, **6**(114), 113630–113647.

53 K. L. Pan, C. W. Young, G. T. Pan and M. B. Chang, Catalytic reduction of NO by CO with Cu-based and Mn-based catalysts, *Catal. Today*, 2020, **348**, 15–25.